14th International Symposium on Turbulence and Shear Flow Phenomena (TSFP14)
Heidelberg, Germany, July 28–31, 2026

EFFECT OF MANIPULATING LOGARITHMIC LAW ON FRICTION DRAG REDUCTION IN A TURBULENT CHANNEL FLOW

Yusuke Nabae
Department of Mechanical Systems Engineering
Tokyo Metropolitan University
6-6 Asahigaoka, Hino-shi, Tokyo 191-0065, Japan
nabae-yusuke@tmu.ac.jp

Hiroya Mamori
Department of Mechanical and Intelligent Systems
The University of Electro-Communications
1-5-1 Chofugaoka, Chofu, Tokyo 182-8585, Japan
mamori@uec.ac.jp

Hiroshi Gotoda
Department of Mechanical Engineering
Tokyo University of Science
6-3-1 Niijuku, Katsushika-ku,
Tokyo 125-8585, Japan
gotoda@rs.tus.ac.jp

Koji Fukagata
Department of Mechanical Engineering
Keio University
3-14-1 Hiyoshi, Kohoku-ku,
Yokohama, Kanagawa 223-8522, Japan
fukagata@mech.keio.ac.jp

ABSTRACT

We theoretically and numerically investigate the effect of manipulating the logarithmic law in the mean velocity profile on the drag reduction effect in a fully developed turbulent channel flow under a constant pressure gradient condition. According to the theoretical analysis of the mean velocity profile, not only the suppression of near-wall turbulence, which results in increasing the integration constant B and whose effect mildly decreases with Re_τ, but also decreasing the Kármán constant κ is valid for achieving significant drag reduction in turbulent flows at practically high Reynolds numbers. Subsequently, we conduct direct numerical simulation (DNS) of a turbulent channel flow controlled by damping the spanwise velocity fluctuations, i.e., the idealized w-damping control to investigate in what conditions κ actually changes. The present DNS results support the hypothesis obtained from the theoretical analysis: the decrease in the Kármán constant may correspond to the suppression of Reynolds shear stress in the region far from the wall.

INTRODUCTION

Skin-friction drag reduction is of great importance for solving various environmental issues such as depletion of energy resources. Many flow control techniques for the friction drag reduction have been proposed (e.g., Kasagi et al., 2009; Ricco et al., 2021; Fukagata et al., 2024). In some flow control methods, the drag reduction rate at practically high Reynolds numbers, i.e., $Re_\tau \sim 10^5$–10^6 (Re_τ is the friction Reynolds number), has been predicted based on a theoretical analysis (Iwamoto et al., 2005) or the results obtained by a direct numerical simulation (DNS) of low-Reynolds-number turbulent channel flow (Gatti and Quadrio, 2016; Nabae et al., 2020). Recently, a large-eddy simulation has been utilized to investigate the drag reduction effect in wall-bounded flows at relatively high Reynolds numbers, i.e., $Re_\tau \sim 10^3$–10^4 (Marusic et al., 2021; Nabae et al., 2025). According to their predictions, the drag reduction rate mildly decreases as the Reynolds number increases, so that the substantial drag reduction effects can be expected even at practically high Reynolds numbers. However, it is still not fully answered what flow control strategies are valid for achieving the substantial drag reduction at practically high Reynolds numbers.

Based on this background, to establish the flow control strategy which is effective in the wide range of the Reynolds numbers up to practically high Reynolds numbers, we theoretically investigate the effect of manipulating the logarithmic law in the mean velocity profile on the drag reduction effect in a fully developed turbulent channel flow under a constant pressure gradient (CPG) condition. Subsequently, as a complementary investigation, we perform the DNS of a fully developed turbulent channel flow controlled by damping the spanwise velocity fluctuations (Frohnapfel et al., 2010).

THEORETICAL ANALYSIS

Throughout the paper, all variables are made dimensionless by the fluid density ρ^*, the friction velocity u_τ^*, and the channel half-width δ^*, where the superscript * represents dimensional quantities. The subscript 1, 2, and 3 denote the streamwise, wall-normal, and spanwise directions, respectively. In addition, u_i $(i = 1, 2, 3)$, p, and t denote the velocity components, pressure, and time, respectively. Here, for convenience, (x_1, x_2, x_3) and (u_1, u_2, u_3) are interexchangably denoted by (x, y, z) and (u, v, w), respectively. The friction Reynolds number is defined as $Re_\tau = \delta^* u_\tau^* / \nu^*$, where ν^* is the kinematic viscosity.

We first model the mean velocity profile in a fully developed turbulent channel flow to investigate the effect of manipulating the logarithmic law in the mean velocity profile on the drag reduction effect. To enable us to systematically change not only the Kármán constant κ but also the integral constant B, we propose the model combining the turbulent viscosity model proposed by Reynolds and Tiederman (1967) U^+_{RT} and the logarithmic law $U^+_{\log}$:

$$U^+_{\mathrm{model}}\left(y^+\right) = (1-\gamma)\cdot U^+_{\mathrm{RT}}\left(y^+\right) + \gamma \cdot U^+_{\log}\left(y^+\right), \quad (1)$$

where superscript + represents the wall unit. For the concrete expression of U^+_{RT}, readers are referred to Reynolds and Tiederman (1967). The logarithmic law $U^+_{\log}$ is modeled as

$$U^+_{\log}\left(y^+\right) = \left(1 - E\left(y^+\right)\right) \cdot \left(\frac{1}{\kappa}\ln y^+ + B\right) + E\left(y^+\right) \cdot U^+_c, \tag{2}$$

where $E\left(y^+\right)$ and U_c are utilized for the law of the wake by Krug et al. (2017). Finally, to smoothly connect U^+_{RT} and $U^+_{\log}$, we adopt the damping function (Hwang and Cossu, 2010), i.e.,

$$\gamma\left(y^+\right) = 1 - \exp\left[-\left(y^+/25\right)^3\right]. \tag{3}$$

In this study, we perform a parametric study of the Kármán constant κ and the integral constant B in Eq. (2) to investigate the effect of manipulating the logarithmic law on the drag reduction effect. Note that we utilize $\kappa = 0.384$ and $B = 4.27$ in the uncontrolled case, which are the same as those proposed by Lee and Moser (2015).

In this study, the drag reduction rate R_D is defined as $R_D = \left(C_{f0} - C_f\right)/C_{f0}$, where C_{f0} and $C_f = 2/U_b^{+2}$ are the friction drag coefficient in the uncontrolled and controlled cases, respectively. Since the bulk Reynolds number $Re_b = 2U_b^*\delta^*/\nu^*$ in the CPG condition is changed by the control, C_{f0} at the resultant bulk Reynolds number of the controlled flow is calculated using the approximate formula between the bulk Reynolds number Re_b and the bulk-mean velocity of the uncontrolled flow based on the Reynolds–Tiederman model (Reynolds and Tiederman, 1967) $U^+_{b,\mathrm{NC}}$, i.e., $U^+_{b,\mathrm{NC}} = 5.1904\log Re_b - 3.6741$, which is the same as the previous studies (Nabae et al., 2020; Nabae et al., 2025).

Table 1 shows the comparison between the bulk-mean velocity U_b^+ computed by Eq. (1) and that obtained by the DNS (Yamamoto and Tsuji, 2018) in the uncontrolled flow. The bulk-mean velocity U_b^+ computed by Eq. (1) is in good agreement with that obtained by the DNS (Yamamoto and Tsuji, 2018). Therefore, the model proposed in this study can well reproduce the mean velocity profile in a turbulent channel flow.

Figure 1 shows the mean velocity profile in the uncontrolled case and the case where the Kármán constant κ or the integral constant B is manipulated. In addition, Fig. 2 shows the drag reduction rates as a function of the friction Reynolds number Re_τ. As shown in Fig. 1(a), the increase in B results in the upward shift of the mean velocity profile in the logarithmic region, which corresponds to the extension of the region where the mean velocity profile follows the linear law, i.e., $U^+ = y^+$. Figure 2(a) shows that the drag reduction rate R_D in the case where B is manipulated mildly decreases as Re_τ increases regardless of B. This trend for R_D is similar to that observed in the previous studies applying the idealized damping near the wall (Iwamoto et al., 2005) and streamwise traveling waves of spanwise wall motion (Gatti and Quadrio, 2016), which are the flow control strategies manipulating the near-wall turbulence. Thus, it is implied that the increase in B corresponds to the extension of the viscous sublayer owing to the suppression of turbulent structures near the wall.

In the case where κ is manipulated, shown in Figs. 1(b) and 2(b), the decrease in κ (i.e., the increase in $1/\kappa$) leads to the increase in the slope of the logarithmic region. In addition, we observe the trend of R_D opposite to that observed in the case where B is manipulated: R_D mildly increases with Re_τ. This is because the increase in the slope of the logarithmic region results in the significant upward shift of the logarithmic law in the region near the channel center. Considering Prandtl's mixing length theory, the decrease in κ may correspond to the suppression of Reynolds shear stress (RSS) far from the wall. However, this hypothesis is still controversial.

In summary, these results suggest that the flow control strategy for not only increasing the integral constant B (i.e., the suppression of near-wall turbulence) but also decreasing the Kármán constant κ is valid for achieving the substantial drag reduction in the wide range of Reynolds numbers up to practically high Reynolds numbers, i.e., $Re_\tau \sim 10^5$–10^6.

DIRECT NUMERICAL SIMULATION

To investigate in what conditions κ actually changes, we perform the DNS of a fully developed turbulent channel flow controlled by damping the spanwise velocity fluctuations, i.e., the idealized w-damping control (Frohnapfel et al., 2010). The governing equations are the incompressible continuity and Navier–Stokes equations, i.e.,

$$\frac{\partial u_i}{\partial x_i} = 0, \tag{4}$$

$$\frac{\partial u_i}{\partial t} = -\frac{\partial\left(u_i u_j\right)}{\partial x_j} - \frac{\partial p}{\partial x_i} + \frac{1}{Re_\tau}\frac{\partial^2 u_i}{\partial x_j \partial x_j} - \frac{dP}{dx_1}\delta_{i1} + f_b\delta_{i3}. \tag{5}$$

The friction Reynolds number is set to $Re_\tau = 590$ and 1000 in this study. Similarly to Frohnapfel et al. (2010), we apply the idealized w-damping control to the region near the upper and lower walls, i.e., $0 \le y^+ \le y_d^+$ and $2Re_\tau - y_d^+ \le y^+ \le 2Re_\tau$ (y_d^+ is the damping layer thickness), so that the RSS in the damping layer is suppressed by the control. For this control, the body force f_b in Eq. (5) is given as $f_b^+ = -w'^+/\Phi^+$, where Φ^+ corresponds to the strength of the forcing: similarly to Iwamoto et al. (2005), $\Phi^+ = 1$ in this study. The damping layer thickness y_d^+ is varied in the region of $5 \le y_d^+ \le 60$. The periodic boundary condition is applied in the streamwise (x) and spanwise (z) directions. The no-slip boundary condition, i.e., $u = v = w = 0$, is imposed on the both walls.

The DNS code used in this study is based on that developed in the previous studies (Fukagata et al., 2006; Nabae and Fukagata, 2024; Nabae et al., 2025). For the spatial discretization, we utilize the energy-conserving fourth-order finite difference scheme (Morinishi et al., 1998) in the streamwise and spanwise directions and second-order finite difference scheme in the wall-normal direction. The time integration is conducted by the low-storage, third-order Runge-Kutta/Crank-Nicolson scheme (Spalart et al., 1991) with the high-order SMAC-like velocity-pressure coupling scheme (Dukowicz and Dvinsky, 1992). The pressure Poisson equation is solved using a two-dimensional fast Fourier transform in the streamwise and spanwise directions and using the tridiagonal matrix algorithm in the wall-normal direction. The computational conditions are summarized in table 2, where L_i, N_i, and Δx_i denote the length of the computational domain, the number of grid points, and the grid spacing, respectively, in the i–th direction.

Figure 3 compares the RSS and the diagnostic function, i.e.,

$$\frac{1}{\kappa} = y^+\frac{dU^+}{dy^+}, \tag{6}$$

Table 1. Comparison between U_b^+ computed by Eq. (1) and that obtained by the DNS (Yamamoto and Tsuji, 2018).

Re_τ	1000	2000	4000	8000
Proposed model of Eq. (1)	19.9	21.7	23.5	25.3
DNS (Yamamoto and Tsuji, 2018)	19.9	21.8	23.4	25.0

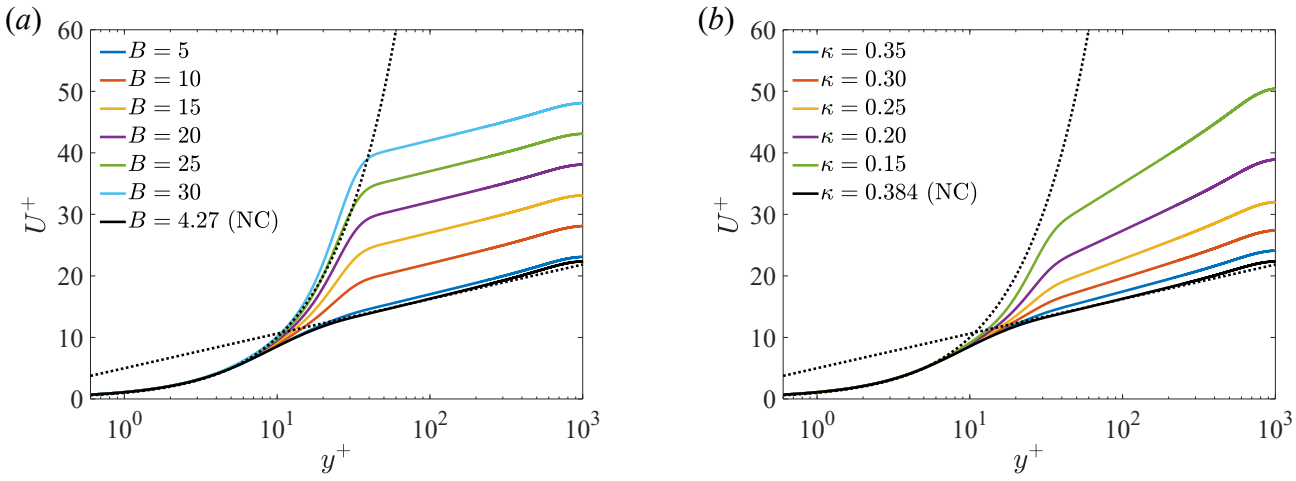

Figure 1. Comparison of modeled mean velocity profiles in the uncontrolled and controlled cases: (*a*) the cases where the integral constant B is manipulated; (*b*) the cases where the Kármán constant κ is manipulated.

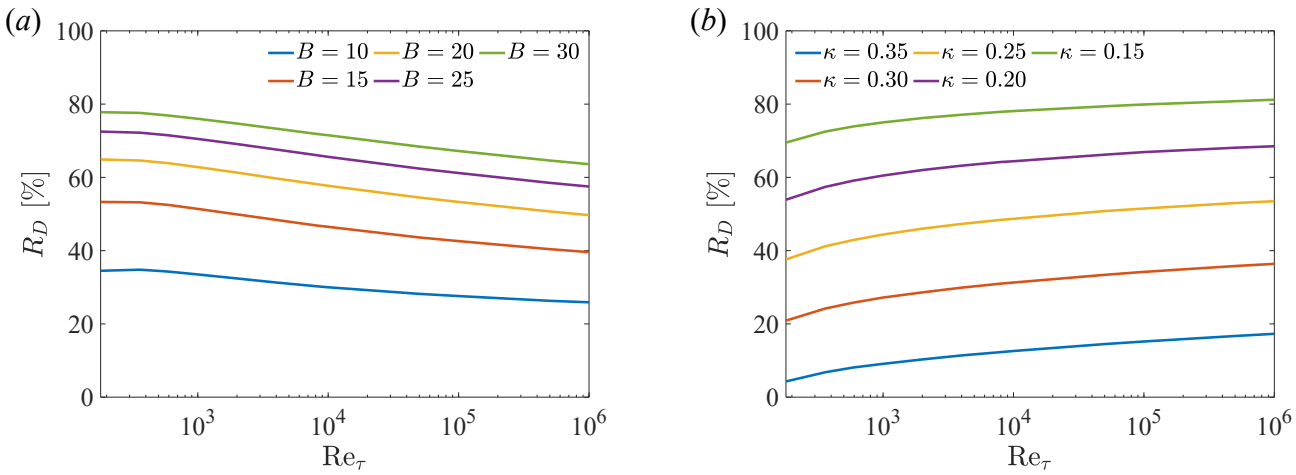

Figure 2. Drag reduction rate R_D as a function of the friction Reynolds number Re_τ: (*a*) the cases where the integral constant B is manipulated; (*b*) the cases where the Kármán constant κ is manipulated.

Table 2. Computational conditions in the present DNS.

Re_τ	$L_x \times L_y \times L_z$	$N_x \times N_y \times N_z$	Δx^+	Δy^+	Δz^+
590	$384 \times 256 \times 384$	$2\pi \times 2 \times \pi$	9.7	0.9–7.6	4.8
1000	$512 \times 384 \times 512$	$2\pi \times 2 \times \pi$	11.1	0.7–8.8	6.1

in the uncontrolled and controlled cases at $Re_\tau = 590$. As shown in Fig. 3(*a*), we observe the extension of the region where the RSS is suppressed as the damping layer thickness increases. Focusing on the diagnostic function of Eq. (6), in the case where the damping layer thickness y_d^+ is in the viscous sublayer, i.e., $y_d^+ = 5$, the Kármán constant is hardly changed, whereas in the case of $y_d^+ \geq 10$, the increase in the damping layer thickness leads to the increase in $1/\kappa$, i.e., the decrease in κ. These results imply that the suppression of RSS far from the wall leads to the decrease in the Kármán constant. For example, in the case of $y_d^+ = 50$, we can obtain $\kappa = 0.269$ ($1/\kappa = 3.712$) and $B = 35.2$ from the DNS results. Using Eq. (1) with $(\kappa, B) = (0.269, 35.2)$, the drag reduction rate of $R_D = 84.6\%$ is predicted at $Re_\tau = 590$, which is in reasonable

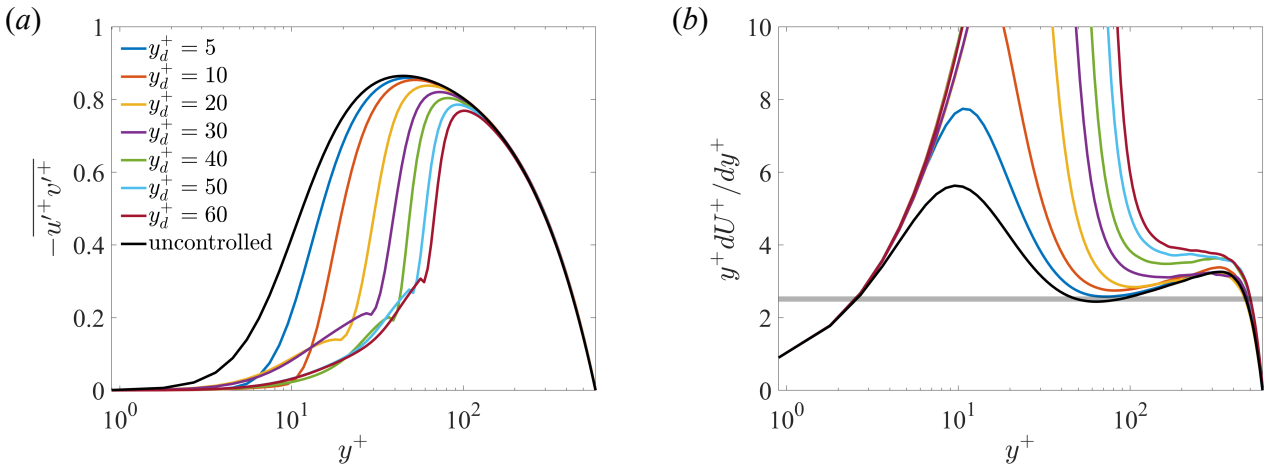

Figure 3. Comparison of (*a*) RSS and (*b*) Eq. (6) in the uncontrolled and controlled cases at $Re_\tau = 590$. Grey region in (*b*) represents the value in the uncontrolled case, i.e., $0.387 \leq \kappa \leq 0.41$.

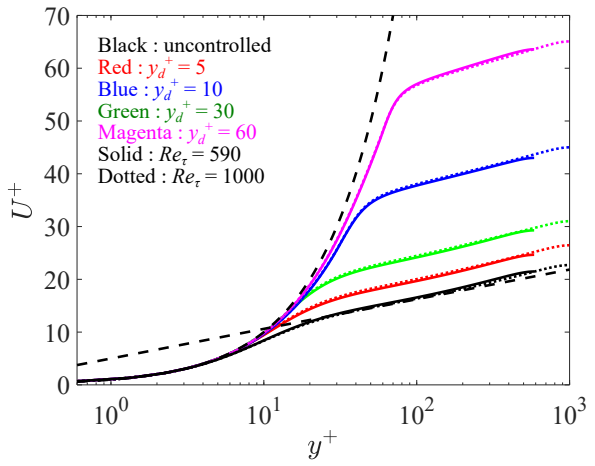

Figure 4. Reynolds number effect on the mean velocity profile in the cases of $y_d^+ = 5$, 10, 30, and 60 at $Re_\tau = 590$ and 1000.

agreement with that obtained by the DNS, i.e., $R_D = 84.1\%$.

Figure 4 shows the Reynolds number effect on the mean velocity profile in the cases of $y_d^+ = 5$, 10, 30, and 60 at $Re_\tau = 590$ and 1000. Regardless of the damping layer thickness y_d^+, the mean velocity profiles at $Re_\tau = 590$ and 1000 are found to be in reasonable agreement, implying that the modeling of the mean velocity profile at $Re_\tau = 590$ can well predict the drag reduction rate in the wide range of the Reynolds numbers.

Figure 5 shows the Kármán constant κ and the integral constant B obtained from the DNS results in the cases of $y_d^+ = 5$, 10, 30, and 60 at $Re_\tau = 590$ and 1000. Note that "$y_d^+ = 0$" corresponds to the uncontrolled case. The increase in the damping layer thickness, i.e., the increase in the drag reduction rate, leads to the decrease in the Kármán constant κ and the increase in the integral constant B, which correspond to the increase in the slope of the logarithmic law and the vertical shift of the logarithmic law, respectively. In the case where the damping layer thickness is in the viscous sublayer, i.e., $y_d^+ = 5$, the Kármán constant κ is in reasonable agreement with that of the uncontrolled flow, whereas the damping of the RSS in the very near-wall region slightly increases the integral constant B. In th case where the damping layer thickness reaches the buffer and logarithmic layers, i.e., $y_d^+ \geq 10$, the Kármán constant and the integral constant is significantly decreased and increased by the control, respectively. This is because the damping of the spanwise velocity fluctuations in the wide region from the viscous sublayer to the logarithmic layer significantly suppresses not only the RSS near the wall, i.e., the near-wall turbulence, but also the RSS far from the wall. These results are basically in line with the trends by the theoretical analysis.

Figure 6 shows the comparison between the drag reduction rates obtained from the DNS and those predicted by Eq. (1). Note that we utilize the Kármán constant κ and the integral constant B obtained from the DNS at $Re_\tau = 590$ to predict the drag reduction rate through Eq. (1). Regardless of the damping layer thickness, the drag reduction rates obtained by the present DNS is in good agreement with those predicted by the proposed model. In the case where the damping layer thickness is relatively large, i.e., $y_d^+ \geq 30$, large drag reduction rate remains in the wide range of the Reynolds numbers. This DNS result supports the finding obtained from the theoretical analysis: the flow control strategy for not only increasing the integral constant B (i.e., the suppression of near-wall turbulence) but also decreasing the Kármán constant κ (i.e., the decrease in the RSS far from the wall) is valid for achieving the substantial drag reduction in the wide range of Reynolds numbers up to practically high Reynolds numbers, i.e., $Re_\tau \sim 10^5$–10^6.

CONCLUSIONS

We have theoretically and numerically investigated the effect of manipulating the logarithmic law in the mean velocity profile on the drag reduction effect in a fully developed turbulent channel flow. According to the theoretical analysis of the mean velocity profile, in the case where the Kármán constant in the logarithmic law is manipulated, the drag reduction rate mildly increases as the friction Reynolds number increases. While the increase in the integral constant corresponds to the vertical shift of the logarithmic law, the decrease in the Kármán constant corresponds to the increase in the slope of the logarithmic law. These manipulations result in a drag reduction effect. Subsequently, we conduct direct numerical simulation (DNS) of a turbulent channel flow controlled by damping the spanwise velocity fluctuations, i.e., the idealized *w*-damping control. The present DNS results support the hypothesis obtained from the theoretical analysis: the decrease in the Kármán constant may correspond to the suppression of Reynolds shear stress in the region far from the wall. The re-

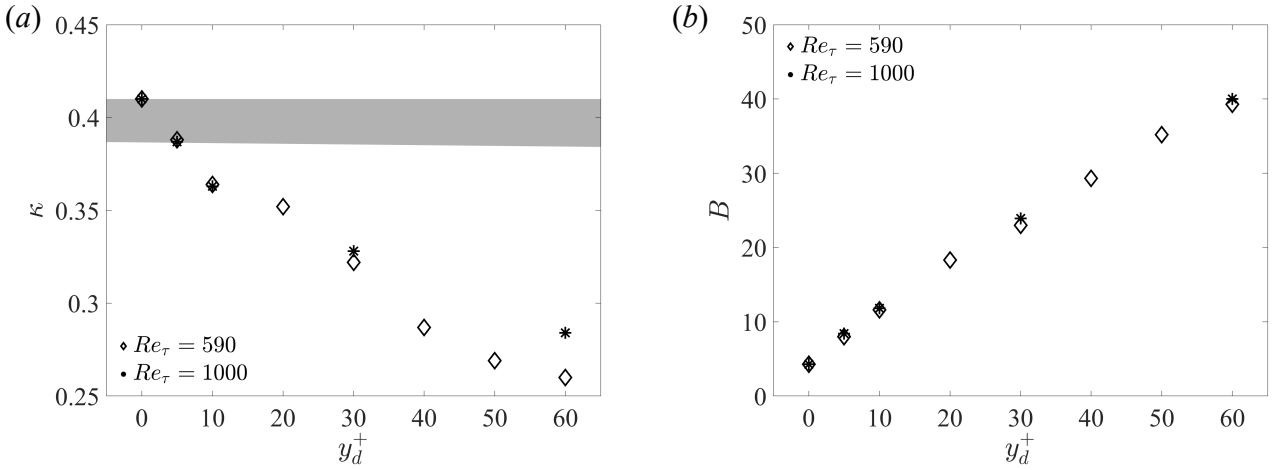

Figure 5. (*a*) Kármán constant κ and (*b*) integral constant B obtained from the DNS results in the cases of $y_d^+ = 5$, 10, 30, and 60 at $Re_\tau = 590$ and 1000.

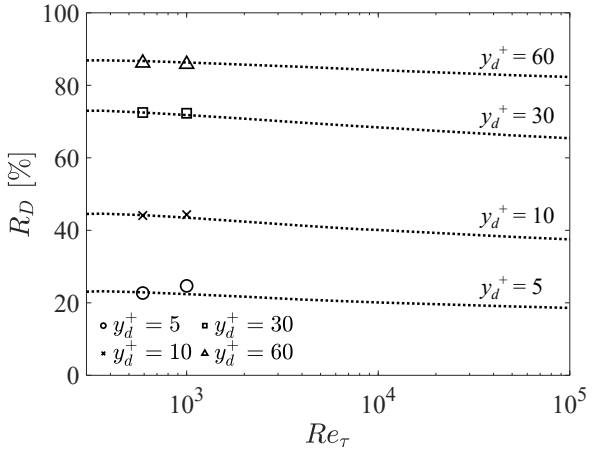

Figure 6. Comparison between the drag reduction rates obtained from the DNS and those predicted by Eq. (1). Here, we apply the Kármán constant κ and the integral constant B obtained from the DNS at $Re_\tau = 590$ to Eq. (2).

sults obtained in this study imply that the flow control strategy not only increasing the integral constant B (i.e., the suppression of near-wall turbulence) but also decreasing the Kármán constant κ (i.e., the suppression of Reynolds shear stress in the region far from the wall) is valid for achieving significant drag reduction in turbulent flows at practically high Reynolds numbers.

ACKNOWLEDGMENTS

Authors are grateful to Dr S. Ogata (Tokyo Metropolitan University) for fruitful discussions. This work was supported through JSPS KAKENHI grant No. 21H05007 and 25K17542 by Japan Society for the Promotion of Science.

REFERENCES

Dukowicz, J. K. and Dvinsky, A. S. 1992 Approximate factorization as a high order splitting for the implicit incompressible flow equations. *Journal of Computational Physics* **102**, 336–347.

Frohnapfel, B., Hasegawa, Y., and Kasagi, N. 2010 Friction drag reduction through damping of the near-wall spanwise velocity fluctuation. *International Journal of Heat and Fluid Flow* **31**, 434–441.

Fukagata, K., Kasagi, N., and Koumoutsakos, P. 2006 A theoretical prediction of friction drag reduction in turbulent flow by superhydrophobic surfaces. *Physics of Fluids* **18**, 051703.

Fukagata, K., Iwamoto, K., and Hasegawa, Y. 2024 Turbulent drag reduction by streamwise traveling waves of wall-normal forcing. *Annual Review of Fluid Mechanics* **56**, 69–90.

Gatti, D. and Quadrio, M. 2016 Reynolds-number dependence of turbulent skin-friction drag reduction induced by spanwise forcing. *Journal of Fluid Mechanics* **802**, 553–582.

Hwang, Y. and Cossu, C. 2010 Self-sustained process at large scales in turbulent channel flow. *Physical Review Letters* **105**, 044505.

Iwamoto, K., Fukagata, K., Kasagi, N., and Suzuki, Y. 2005 Friction drag reduction achievable by near-wall turbulence manipulation at high Reynolds numbers. *Physics of Fluids* **17**, 011702.

Kasagi, N., Suzuki, Y., and Fukagata K. 2009 Microelectromechanical systems–based feedback control of turbulence for skin friction reduction. *Annual Review of Fluid Mechanics* **41**, 231–251.

Krug, D., Philip, J., and Marusic, I. 2017 Revisiting the law of the wake in wall turbulence. *Journal of Fluid Mechanics* **811** 421–435.

Lee, M. and Moser, R. D. 2015 Direct numerical simulation of turbulent channel flow up to $Re_\tau \approx 5200$. *Journal of Fluid Mechanics* **774**, 395–415.

Marusic, I., Chandran, D., Rouhi, A., Fu, M. K., Wine, D., Holloway, B., Chung, D., and Smits, A. J. 2021 An energy-efficient pathway to turbulent drag reduction. *Nature Communication* **12**, 5805.

Morinishi, Y., Lund, T. S., Vasilyev, O. V., and Moin, P. 1998 Fully conservative higher order finite difference schemes for incompressible flow. *Journal of Computational Physics* **143**, 90–124.

Nabae, Y., Kawai, K., and and Fukagata, K. 2020 Prediction of drag reduction effect by streamwise traveling wave-like wall deformation in turbulent channel flow at practically high Reynolds numbers. *International Journal of Heat and Fluid Flow* **82**, 108550.

Nabae, Y. and Fukagata, K. 2024 Theoretical and numerical analyses of turbulent plane Couette flow controlled using uniform blowing and suction. *International Journal of Heat*

and Fluid Flow **106**, 109286.

Nabae, Y., Inagaki, K., Kobayashi, H., Gotoda, H., and Fukagata, K. 2025 Large-eddy simulation of high-Reynolds-number turbulent channel flow controlled using streamwise travelling wave-like wall deformation for drag reduction. *Journal of Fluid Mechanics* **1003**, A2.

Reynolds, W. C. and Tiederman, W. G. 1967 Stability of turbulent channel flow, with application to Malkus's theory. *Journal of Fluid Mechanics* **27**, 253–272.

Ricco, P., Skote, M., and Leschziner, M. A. 2021 A review of turbulent skin-friction drag reduction by near-wall transverse forcing. *Progress in Aerospace Sciences* **123**, 100713.

Spalart, P. R., Moser, R. D. and Rogers, M. M. 1991 Spectral methods for the Navier-寰鉄 tokes equations with one infinite and two periodic directions. *Journal of Computational Physics* **96**, 297–324

Yamamoto, Y. and Tsuji, Y. 2018 Numerical evidence of logarithmic regions in channel flow at $Re_\tau = 8000$. *Physical Review Fluids* **3**, 012602.